Microscopic evidence for strong periodic lattice distortion in two-dimensional charge-density wave systems

Jixia Dai,[1,*] Eduardo Calleja,[1] Jacob Alldredge,[1] Xiangde Zhu,[2] Lijun Li,[3] Wenjian Lu,[3] Yuping Sun,[3,2] Thomas Wolf,[4] Helmuth Berger,[5] and Kyle McElroy[1,†]

[1]*Department of Physics, University of Colorado at Boulder, Boulder, Colorado 80309, USA*

[2]*High Magnetic Field Laboratory, CAS, Hefei 230031, China*

[3]*Key Laboratory of Materials Physics, Institute of Solid State Physics, CAS, Hefei 230031, China*

[4]*Karlsruher Institut für Technologie, Institut für Festkörperphysik, P.O.B. 3640, D-76021 Karlsruhe, Germany*

[5]*Institute of Physics of Complex Matter, Ecole Polytechnique Federal de Lausanne, CH-1015 Lausanne, Switzerland*

(Received 15 March 2014; published 30 April 2014)

In quasi-two-dimensional electron systems of layered transition metal dichalcogenides (TMDs) there is still controversy about the nature of the transitions to charge-density wave (CDW) phases, i.e., whether they are described by a Peierls-type mechanism or by a lattice-driven model. By performing scanning tunneling microscopy experiments on canonical TMD-CDW systems, we image the electronic modulation and the lattice distortion separately in 2H-TaS_2, $TaSe_2$, and $NbSe_2$. Across the three materials, we found dominant lattice contributions instead of the electronic modulation expected from Peierls transitions, in contrast to the CDW states, which show the hallmark of contrast inversion between filled and empty states. Our results imply that periodic lattice distortion plays a vital role in the formation of CDW phases in TMDs and illustrate the importance of taking into account the more complicated lattice degrees of freedom when studying correlated electron systems.

DOI: 10.1103/PhysRevB.89.165140 PACS number(s): 71.45.Lr, 71.27.+a, 74.55.+v

Transition metal dichalcogenides (TMDs) have shown intriguing phenomena like spin-valley physics [1,2], superconductivity induced/enhanced by tuning various parameters [3–9], and charge-density waves (CDWs) that coexist and compete with superconductivity (e.g., 2H-$NbSe_2$, $TaSe_2$, 1T-TaS_2, and $TiSe_2$) [5–9]. Such competition between CDWs and superconductivity is closely tied to the complicated interactions between the internal degrees of freedom, including charge, lattice, and orbital. Differentiating which interactions are key requires knowing which of them are responsible for the different phases. The degree to which an electron-driven mechanism is the cause of CDWs in trigonal prismatic structured (2H) TMDs is still under debate. Existing studies have proposed a variety of different mechanisms, including Fermi surface nesting [10,11], saddle-band-driven susceptibility divergence [12], f-wave gapping, marginal Fermi liquid [13], etc.

These materials do show some evidence of the electronic nature of CDW phases including the existence of incommensurate CDW phases [14,15], since $2k_F$ is generally not expected to be a rational fraction of lattice reciprocal vectors. Furthermore, the electronic origin is also supported by photoemission experiments which measured the Fermi surface of $NbSe_2$ and $TaSe_2$ and approximated the electronic susceptibility with an autocorrelation. This analysis showed peaks at wave vectors corresponding to those of the CDW [10,11]. However, inelastic an x-ray scattering experiment in $NbSe_2$ [16] revealed that the lattice dynamics exhibit unconventional behavior and hence may dominate the transition. Moreover, recent LDA calculations have shown difficulties with Fermi surface nesting and have suggested that periodic lattice distortion (PLD), instead of electron modulation (eMod), is the essential ingredient [17,18]. In a recent real-space study, Soumyanarayanan *et al.* [19] have shown that there is a close relationship between CDW formation and the local strain related to surface layer buckling in $NbSe_2$. Rossnagel *et al.* have, in addition, argued that the spin-orbit interaction is also important for a $5d$-electron system like $TaSe_2$ [20]. Because of this debate, it is necessary to systematically study the CDWs in TMDs, with the simultaneous measurement of any intrinsic lattice distortion, while spatially resolving the electronic component across this family of compounds.

CDW instability in low-dimensional systems was initially explained by the Peierls mechanism [18,21,22], in which a divergence in electronic response function at a particular wave vector ($2k_F$ for one dimension) results in a periodic charge redistribution in real space. That is, a low-dimensional electronic system can lower its energy by opening an energy gap at the Fermi level, piling up electrons periodically, and reducing its lattice transitional symmetry. As a result of the periodic eMod and the electron-phonon interaction, the lattice itself undergoes a similar modulation, which causes an increase in the lattice elastic energy [22]. As a consequence, with this mechanism the lattice distortion is expected to be minimized, acting like a competing effect [18]. The eMod manifests in a change in the local density of states (LDOS), which shows a periodic increase in the density of electrons with holes modulating with the same period but out of phase with the electrons. This can be shown by calculating the LDOS in real space using the Peierls model [23]. Another way of visualizing this alternating intensity is by using the quantum mechanical sum rule, where the summation of the number of filled and empty states on every lattice site is a constant. This means that wherever there are excess electron states, there must be fewer hole states at the same site. The LDOS calculation we performed also shows this conservation of total states.

*daij@colorado.edu

†Kyle.McElroy@colorado.edu

To investigate the nature of the CDW in these materials we use scanning tunneling microscopy (STM), in which the tunneling current is proportional to the sample's integrated density of states and a matrix element with exponential dependence on the tip-sample distance, $I \sim e^{-2\kappa s}\int_0^{eV} \mathrm{LDOS}(\epsilon)d\epsilon$ [24]. In the constant-current imaging mode, the tunneling current is maintained at a fixed value, with the tip-sample distance being adjusted and recorded. For a CDW system that contains only eMod, and no lattice distortions, the topographic images of the filled and empty states will be complementary with each other due to the nature of LDOS variation and uniformity of atomic heights. This phenomenon has been well demonstrated by STM experiments on the quasi-one-dimensional (quasi-1D) $NbSe_3$ [25], the quasi-2D system $K_{0.9}MoO_3$ [26], and the quasi-2D CaC_6 with 1D modulation [27]. In each of these cases the modulations for filled and empty states, with the CDW periodicity, are of opposite phases in the topography (contrast inversion) as predicted by the Peierls model.

In this study, we have used single-crystal samples of TaS_2, $NbSe_2$, and $TaSe_2$ prepared by the iodine vapor transport method. STM experiments were performed using our home-built systems, including a variable-temperature scanning tunneling microscope (6 to 300 K) and a low-temperature scanning tunneling microscope (5.3 K). In both systems, the samples were cleaved at room temperature in ultrahigh vacuum before being loaded into the scanning tunneling microscope. Etched tungsten tips, prepared *in situ* by field emission against gold surfaces, are used to obtain high-quality tunneling junctions together with spatial resolution at the atomic scale. We examined three 2H-TMDs: TaS_2, $TaSe_2$, and $NbSe_2$. Figure 1(a) is a representative constant current topographic image of a 2H-TaS_2 surface showing both the atomic corrugation and the 3×3 CDW superlattice. Figure 1(b) shows the crystal structure with the neutral cleave plane (dashed line) between the two layers of chalcogen atoms. The atomic lattice shown in Fig. 1(a) is the resulting triangular chalcogen lattice, while the evident 3×3 superlattice is due to the formation of the CDW. The Fourier transform [Fig. 1(c)] in Fig. 1(a) shows that the atomic and the CDW signals are the main features of this surface. After excluding the atomic corrugation by Fourier filtering, we find that the height of the top layer of atoms varies of the order of picometer in the z direction due to the formation of the CDW, for all three of the 2H-TMDs. This change is consistent with the distortion measured by both x-ray diffraction [28] and neutron scattering experiments [14], strongly indicating that our surface-sensitive measurements of the CDW show a behavior similar to that seen in the bulk. The strong commensurability between the CDW and the lattice in the STM images agrees well with that measured by scattering experiments. This is in agreement with the strong $\boldsymbol{q}$-dependent electron-phonon interaction's being involved in the CDW of these materials [16].

In order to probe the differences between the filled and the empty states of the CDW phases in these materials topographic images were taken at opposite sample bias voltages. In Figs. 2 and 3, our topographic images obtained for 2H-TaS_2, $NbSe_2$, and $TaSe_2$ are shown. Figures 2(a) and 2(b) are images of the filled and empty states (as indicated by negative and positive

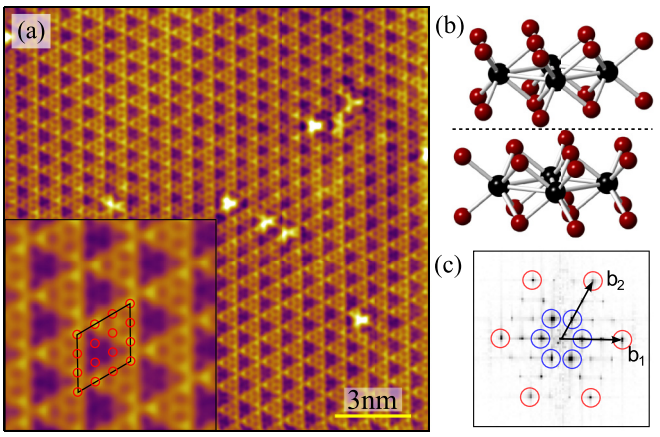

FIG. 1. (Color online) (a) Atomically resolved topographic image of 2H-TaS_2 with CDW modulation (3×3 superstructure). This image was obtained at 60 K and with setup conditions of -100 mV and 200 pA. Inset: Zoom-in showing the atomic structure of the 3×3 unit cell, with lighter (red) spheres indicating sulfur atoms. (b) Crystal structure of trigonal prismatic (2H) TMD. Lighter (red) spheres are chalcogen atoms; black spheres, metal atoms. The dotted horizontal line is where it cleaves. (c) Fourier transform of (a). Inner (blue) circles [outer (red) circles] indicate the primary peaks of CDW [atomic] modulation, and $\boldsymbol{b_1}$ and $\boldsymbol{b_2}$ are the atomic lattice reciprocal vectors.

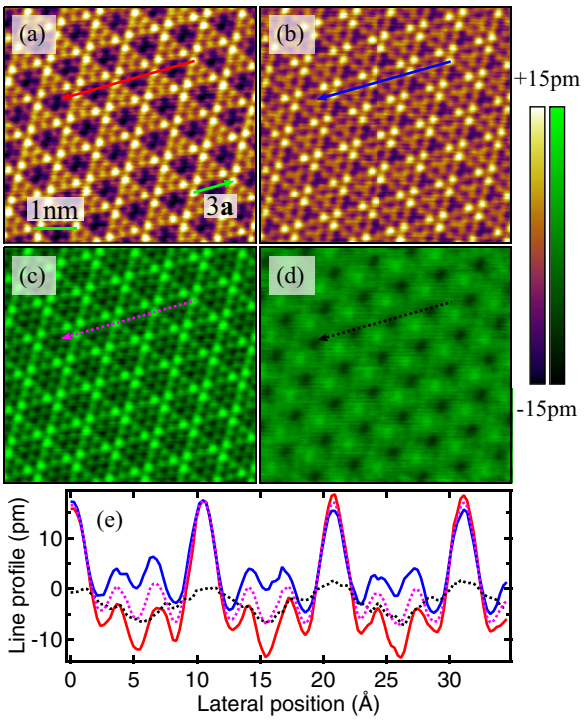

FIG. 2. (Color online) Topographic images showing symmetrization and antisymmetrization on 2H-TaS_2 at 52 K: (a) -50 mV and 100 pA; (b) $+50$ mV and 100 pA. These two images were individually corrected for drift and aligned with subatomic precision. (c, d) Symmetrized [$S = (a + b)/2$] and antisymmetrized [$AS = (a - b)/2$] images of (a) and (b). The contrast in (d) is much smaller compared to (c). (e) Line profiles in (a–d) indicated by colors.

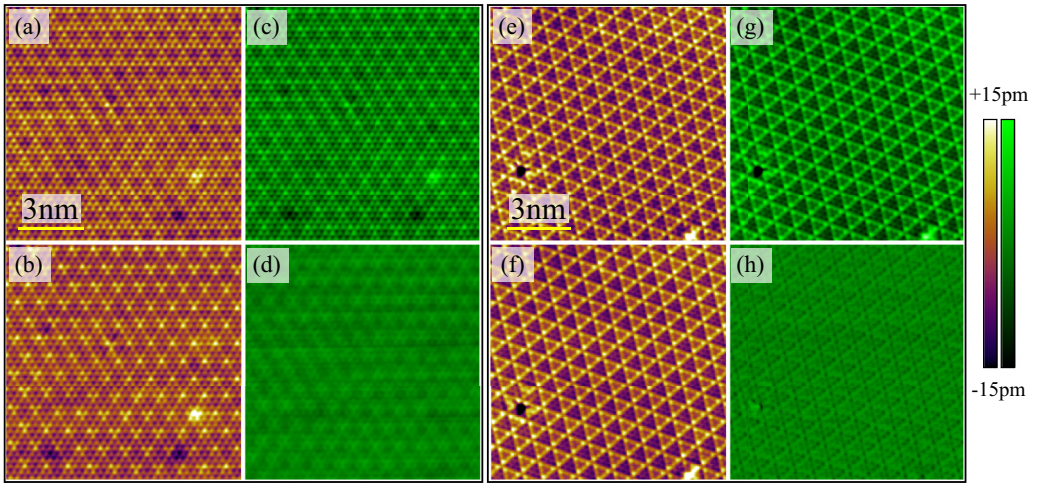

FIG. 3. (Color online) Topographic images of $NbSe_2$ and $TaSe_2$ at 5 K. (a, b) $NbSe_2$ with −100 mV and 100 pA (a) and with +100 mV and 100 pA (b). (e, f) $TaSe_2$ with −50 mV and 40 pA (e) and with +50 mV and 30 pA (f). (c, g) Symmetrized and antisymmetrized images of (a, e); (d, h) symmetrized and antisymmetrized images of (b, f). The contrast of (c, g) is much larger than that of (d, h), as for TaS_2.

sample biases) in TaS_2, while Figs. 3(a), 3(b), 3(e), and 3(f) are images of the empty and filled states in $NbSe_2$ and $TaSe_2$. Prior to analysis, these images are processed with a drift-correction algorithm [29] so that images taken at different times can be aligned on a subatomic length scale. Surface defects are used to ensure accuracy of the drift correction algorithm. For images of TaS_2, line subtraction is applied to remove a low-frequency vibrational noise. This process, combined with the high thermal stability of our experiment, allows for an extremely precise measurement of position (with less than 50 pm of drift per day) and enables us to uncover the true structure of the CDW state in these materials for the first time.

Comparing our results with those from known CDW systems [25–27], which include STM results on $NbSe_2$ [30], we find qualitative discrepancies. In our measurements, the filled-/empty-state topographic images of the TMD samples do not show the expected out-of-phase or contrast inversion that the Peierls model predicts. This contrasts with previous observations of CDW systems under STM imaging. Instead, the topographic images taken at +50- and −50-mV sample bias voltages on TaS_2 are very similar to each other when one compares them with the naked eye. In order to rigorously check this similarity, we have calculated the normalized cross correlation coefficients (NCCs) between the two images, $\mathrm{NCC} = \langle (a_{ij} - \bar{a})(b_{ij} - \bar{b}) \rangle / (\sigma_a \sigma_b)$, where μ and σ are the mean and the standard deviation of the two images (a_{ij} and b_{ij}). NCC is expected to be +1 for two identical images and −1 for two images with perfect contrast inversion. For an eMod-dominating CDW, where spatial inversion between filled and empty states is expected, one would expect the NCC between the filled- and the empty-state images to be close to −1. What we find when we carry out this analysis on TaS_2, $NbSe_2$, and $TaSe_2$ is that the NCCs are +0.62, +0.79, and +0.95, respectively, showing that the majority of the topographic images are in-phase between the two biases. Considering that only the CDW corrugation will be out-of-phase, while the atomic corrugation is actually in-phase, we can remove the atomic signals by Fourier filtering them and keep only the CDW signal. After removing the atomic signals, the measured NCCs are still +0.37, +0.67, and +0.97 for TaS_2, $NbSe_2$, and $TaSe_2$, respectively, in sharp contrast to the −1 expected for a traditional CDW. It is important to note that this result differs from previous STM results on $NbSe_2$ [30], where spatially out-of-phase electron and hole components were seen. This discrepancy is due to our superior ability to control and correct for drift at the subatomic level.

Interestingly, our measured positive-valued NCCs do not agree with the conventional pure electronic CDW model [22] and instead show that there is another nonelectronic, lattice effect that is important to the formation of the 2D CDW in TMDs. PLD is a natural explanation for the positive NCCs since STM measurement is a combination of the atomic structure (via the tip-sample distance) and the integrated density of states. If the ionic cores, around which the valence electron clouds are centered, are displaced with the CDW transition, i.e., lattice distortion occurs, then the filled-state and empty-state topographic images will be in-phase with each other. This is because they only enter into the tunneling current through the electron-hole symmetric matrix element. In other words, if there is only a periodic lattice distortion, then the filled-state and empty-state topographic images will be the same, except for a possible difference in the amplitudes of the height profiles, which will not affect the NCC. The expected behavior of a PLD dominates what we see in our STM images of 2H-TMDs.

By calculating the symmetrized [Figs. 2(c), 3(c), and 3(g); $S = (a + b)/2$, where a and b are the images of filled and empty states] and antisymmetrized [Figs. 2(d), 3(d), and 3(h), $AS = (a - b)/2$] images, we can directly access the PLD and eMod parts of the data, respectively [31]. Results of these calculations, shown in Figs. 2 and 3 using the same height scaling, clearly show that the symmetrized channel has a larger z range than that of the antisymmetrized channel, agreeing with our measured NCCs above. The two channels (S and AS) reveal the decomposed, spatially resolved, PLD and eMod components of the 3×3 superlattice for the first time. We find similar signals for the two other members of the 2H family that we have measured, $NbSe_2$ and $TaSe_2$. In the framework

of Peierls instability, the lattice distortion acts as a secondary effect which has to be minimized because it increases the elastic energy of the ground state. Contrasting with the results of the previous STM study [30], we have demonstrated that PLD plays an important, if not the primary, role in CDW formation in 2H-TMDs. This suggests a strong entanglement of the PLD and the eMod, which is not expected in a purely electronic Peierls picture.

Our results agree with the calculations, which show that, without lattice involvement, a CDW cannot exist in these systems. It has long been argued that, without lattice distortions, electron correlations are too strong for a purely electronic CDW to form [32] and that there must be corresponding lattice distortions. Our observations clearly show that these lattice distortions are present and dominate the observed structure in 2H-TMDs, which is in contrast to previous reports [30]. In addition, recent theoretical calculations in this family of materials have shown that the observed CDW vectors do not correspond to the peaks in electronic susceptibility [17]. This calls for a more complicated model that includes nontrivial phonon involvement. Such complicated origins of the charge ordering transition in this simple family of materials demonstrates the necessity of taking the lattice contribution into account in describing the phase diagrams of everything from simple systems like TMDs to more complex correlated electron materials like cuprates and manganites.

The symmetrization process rejects the antisymmetric eMod signal [33] while retaining the PLD contribution, since it enters the images of both the filled and the empty states. It is possible, however, that the antisymmetrized images do contain more information than just that of eMod. In this sense, more quantitative modeling, such as first-principle calculations, would be necessary to compare the relative intensities of PLD and eMod that we present here. As mentioned earlier, the topography is only sensitive to the energy window which is set by the tunneling bias voltage ($\pm$25 to 200 mV in our experiments), so higher energy studies might reveal a more complete picture of CDW in 2H-TMD. Nonetheless, our study provides strong evidence that the 2D CDWs in trigonal prismatic dichalcogenides go beyond the conventional Peierls picture.

In conclusion, we have demonstrated the importance of high-resolution, high-stability, low-drift STM for the understanding of the structure and origins of CDWs in TMDs. We have shown that atomic length scale measurements are necessary in order to resolve and separate the structures of both PLD and eMod in TaS_2, $NbSe_2$, and $TaSe_2$. This shows that PLD dominates the CDW transition for the entire family of 2H-TMDs and that eMod, which has previously been seen as the dominating mechanism, plays a secondary role instead. Our results indicate that a weak-coupling, electron-driven CDW is unlikely to exist in 2H-TMDs and that PLD plays an important role, which is in excellent qualitative agreement with recent theoretical studies [18] and provides quantitative benchmarks to refine our understanding.

The authors thank Dmitry Reznik, Dan Dessau, Yue Cao, and Ray Osborn for useful discussions. K.M. acknowledges support from the A. P. Sloan Foundation. Y.S. and W.L. acknowledge support from National Key Basic Research Grant No. 2011CBA00111 and Joint Funds of the National Natural Science Foundation of China and the Chinese Academy of Sciences' Large-Scale Scientific Facility (Grant No. U1232139).

[1] D. Xiao, G.-B. Liu, W. Feng, X. Xu, and W. Yao, Phys. Rev. Lett. **108**, 196802 (2012).
[2] S. Wu, J. S. Ross, G.-B. Liu, G. Aivazian, A. Jones, Z. Fei, W. Zhu, D. Xiao, W. Yao, D. Cobden, and X. Xu, Nature Phys. **9**, 149 (2013).
[3] J. T. Ye, Y. J. Zhang, R. Akashi, M. S. Bahramy, R. Arita, and Y. Iwasa, Science **338**, 1193 (2012).
[4] K. Taniguchi, A. Matsumoto, H. Shimotani, and H. Takagi, Appl. Phys. Lett. **101**, 042603 (2012).
[5] B. Sipos, A. F. Kusmartseva, A. Akrap, H. Berger, L. Forró, and E. Tutis, Nat. Mater. **7**, 960 (2008).
[6] E. Morosan, H. W. Zandbergen, B. S. Dennis, J. W. G. Bos, Y. Onose, T. Klimczuk, A. P. Ramirez, N. P. Ong, and R. J. Cava, Nature Phys. **2**, 544 (2006).
[7] K. E. Wagner, E. Morosan, Y. S. Hor, J. Tao, Y. Zhu, T. Sanders, T. M. McQueen, H. W. Zandbergen, A. J. Williams, D. V. West, and R. J. Cava, Phys. Rev. B **78**, 104520 (2008).
[8] L. Li, Y. Sun, X. Zhu, B. Wang, X. Zhu, Z. Yang, and W. Song, Solid State Commun. **150**, 2248 (2010).
[9] R. Friend and A. Yoffe, Adv. Phys. **36**, 1 (1987).
[10] S. V. Borisenko, A. A. Kordyuk, A. N. Yaresko, V. B. Zabolotnyy, D. S. Inosov, R. Schuster, B. Büchner, R. Weber, R. Follath, L. Patthey, and H. Berger, Phys. Rev. Lett. **100**, 196402 (2008).
[11] S. V. Borisenko, A. A. Kordyuk, V. B. Zabolotnyy, D. S. Inosov, D. Evtushinsky, B. Büchner, A. N. Yaresko, A. Varykhalov, R. Follath, W. Eberhardt, L. Patthey, and H. Berger, Phys. Rev. Lett. **102**, 166402 (2009).
[12] T. M. Rice and G. K. Scott, Phys. Rev. Lett. **35**, 120 (1975).
[13] A. H. Castro Neto, Phys. Rev. Lett. **86**, 4382 (2001).
[14] D. E. Moncton, J. D. Axe, and F. J. DiSalvo, Phys. Rev. B **16**, 801 (1977).
[15] G. Scholz, O. Singh, R. Frindt, and A. Curzon, Solid State Commun. **44**, 1455 (1982).
[16] F. Weber, S. Rosenkranz, J.-P. Castellan, R. Osborn, R. Hott, R. Heid, K.-P. Bohnen, T. Egami, A. H. Said, and D. Reznik, Phys. Rev. Lett. **107**, 107403 (2011).
[17] M. D. Johannes, I. I. Mazin, and C. A. Howells, Phys. Rev. B **73**, 205102 (2006).
[18] M. D. Johannes and I. I. Mazin, Phys. Rev. B **77**, 165135 (2008).
[19] A. Soumyanarayanan, M. M. Yee, Y. He, J. van Wezel, D. J. Rahn, K. Rossnagel, E. W. Hudson, M. R. Norman, and J. E. Hoffman, Proc. Natl. Acad. Sci. USA **110**, 1623 (2013).
[20] K. Rossnagel and N. V. Smith, Phys. Rev. B **76**, 073102 (2007).
[21] R. E. Peierls, *Quantum Theory of Solids* (Oxford University Press, Oxford, UK, 1955).
[22] G. Grüner, *Density Waves in Solids* (Addison-Wesley Reading, MA, 1994).

[23] See Supplemental Material at http://link.aps.org/supplemental/10.1103/PhysRevB.89.165140 for the detailed LDOS derivation .

[24] C. Chen, *Introduction to Scanning Tunneling Microscopy* (Oxford University Press, New York, 1993).

[25] C. Brun, Z.-Z. Wang, and P. Monceau, Phys. Rev. B **80**, 045423 (2009).

[26] P. Mallet, K. M. Zimmermann, P. Chevalier, J. Marcus, J. Y. Veuillen, and J. M. Gomez Rodriguez, Phys. Rev. B **60**, 2122 (1999).

[27] K. C. Rahnejat, C. A. Howard, N. E. Shuttleworth, S. R. Schofield, K. Iwaya, C. F. Hirjibehedin, C. Renner, G. Aeppli, and M. Ellerby, Nat. Commun. **2**, 558 (2011).

[28] C. D. Malliakas and M. G. Kanatzidis, J. Am. Chem. Soc. **135**, 1719 (2013).

[29] M. J. Lawler, K. Fujita, J. Lee, A. R. Schmidt, Y. Kohsaka, C. K. Kim, H. Eisaki, S. Uchida, J. C. Davis, J. P. Sethna, and E.-A. Kim, Nature (London) **466**, 347 (2010).

[30] P. Mallet, W. Sacks, D. Roditchev, D. Defourneau, and J. Klein, J. Vac. Sci. Technol. B **14**, 1070 (1996).

[31] See Supplemental Material at http://link.aps.org/supplemental/10.1103/PhysRevB.89.165140 for detailed information.

[32] S. K. Chan and V. Heine, J. Phys. F: Metal Phys. **3**, 795 (1973).

[33] See Fig. S2 in Supplemental Material at http://link.aps.org/supplemental/10.1103/PhysRevB.89.165140.